International Journal of Applied Earth Observation and Geoinformation 58 (2017) 36–49

Contents lists available at ScienceDirect

International Journal of Applied Earth Observation and Geoinformation

journal homepage: www.elsevier.com/locate/jag

Evaluation of the global MODIS 30 arc-second spatially and temporally complete snow-free land surface albedo and reflectance anisotropy dataset

Qingsong Sun[a,d,*], Zhuosen Wang[b,c], Zhan Li[a,d], Angela Erb[a], Crystal B. Schaaf[a]

[a] School for the Environment, University of Massachusetts Boston, Boston, MA, USA
[b] NASA Goddard Space Flight Center, Greenbelt, MD, USA
[c] Earth System Science Interdisciplinary Center, University of Maryland College Park, College Park, MD, USA,
[d] Department of Earth and Environment, Boston University, Boston, MA, USA

ARTICLE INFO

Article history:
Received 15 September 2016
Received in revised form
14 December 2016
Accepted 23 January 2017

Keywords:
MODIS
BRDF
Albedo
NBAR
Gap-filling

ABSTRACT

Land surface albedo is an essential variable for surface energy and climate modeling as it describes the proportion of incident solar radiant flux that is reflected from the Earth's surface. To capture the temporal variability and spatial heterogeneity of the land surface, satellite remote sensing must be used to monitor albedo accurately at a global scale. However, large data gaps caused by cloud or ephemeral snow have slowed the adoption of satellite albedo products by the climate modeling community. To address the needs of this community, we used a number of temporal and spatial gap-filling strategies to improve the spatial and temporal coverage of the global land surface MODIS BRDF, albedo and NBAR products. A rigorous evaluation of the gap-filled values shows good agreement with original high quality data (RMSE = 0.027 for the NIR band albedo, 0.020 for the red band albedo). This global snow-free and cloud-free MODIS BRDF and albedo dataset (established from 2001 to 2015) offers unique opportunities to monitor and assess the impact of the changes on the Earth's land surface.

1. Introduction

Land surface albedo, the proportion of incident radiant flux that is reflected, describes the Earth's radiative energy budget and the exchange of radiative energy between the atmosphere and the land surface. The remaining incident radiant flux is absorbed by the Earth and drives land surface processes, such as photosynthesis, plant growth, evaporation, and snow melt. Thus, albedo is an essential climate variable and is required by climate, biogeochemical, hydrological, and weather forecast models at a variety of spatial and temporal scales (Campagnolo et al., 2016; Charney et al., 1977; Dickinson and Hanson, 1984; Lacaze and Maignan, 2006; Lawrence and Chase, 2007a,b, 2010; Martonchik, 1997; Martonchik et al., 2002; Morcrette et al., 2008; Rahman et al., 1993; Schaaf et al., 2002, 2008; Schaaf et al., 2011; Wang et al., 2004, 2016; Zoogman et al., 2016).

Remote sensing provides the only realistic way to capture land surface albedo at a global scale. As multi-angle data from remote sensing sensors such as AVHRR (Advanced Very High Resolution Radiometer), POLDER (POLarization and Directionality of the Earth's Reflectances), MISR (Multi-angle Imaging SpectroRadiometer), MODIS (Moderate-Resolution Imaging Spectroradiometer), and VIIRS (Visible Infrared Imaging Radiometer Suite) have become available, the retrieval of remotely sensed measures of reflectance anisotropy has been adopted as the most flexible method to accurately derive surface albedo (d'Entremont et al., 1999; Diner et al., 2008; Hautecœur and Leroy, 1998; Hu et al., 2000; Leroy et al., 1997; Lucht et al., 2000; Privette et al., 1997; Schaaf et al., 2008, 2011, 2002; Strugnell et al., 2001; Strugnell and Lucht, 2001; Sütterlin et al., 2015; Wanner et al., 1997).

MODIS provides multi-angle observations of each location on the Earth's surface, nearly every day, in order to sample the Bidirectional Reflectance Distribution Function (BRDF) of that location. High quality, cloud-free, directional surface reflectances from both Terra and Aqua are accumulated during 16-day periods and used to derive gridded (500 m) land surface BRDF model parameters, albedo, and NBAR (Nadir-BRDF Adjusted Reflectance) products (Lucht et al., 2002; Schaaf et al., 2002, 2011). These operational

* Corresponding author at: School for the Environment, University of Massachusetts Boston, Boston, MA, USA.
E-mail addresses: qingsong.sun@umb.edu, sqs@bu.edu (Q. Sun).

http://dx.doi.org/10.1016/j.jag.2017.01.011

MODIS products have been available since the launch of Terra in 2000, and have been validated by various rigorous assessment efforts (Cescatti et al., 2012; Liang et al., 2003; Lucht et al., 2000; Román et al., 2010; Salomon et al., 2006; Wang et al., 2012, 2014). The MODIS BRDF products have been used to establish surface vegetation structure and roughness (Chopping et al., 2011; Hill et al., 2011, 2008, 2012; Jiao et al., 2014; Wang et al., 2011). The MODIS albedo products have been used by various modeling communities (Kala et al., 2014; Lawrence and Chase, 2007a,b, 2010; Morcrette et al., 2008; Myhre et al., 2005; Oleson et al., 2003; Roesch et al., 2004; Roy et al., 2016; Wang et al., 2004; Zhou et al., 2003). The NBAR product, and the vegetation indices derived from NBAR, are the primary inputs to the MODIS land cover and phenology products and are also being used for regional crop and range monitoring applications (Friedl et al., 2010; Glanz et al., 2014; Hill et al., 2016; Zhang et al., 2003, 2012, 2002; Zhou et al., 2016).

However, data gaps caused by cloud or ephemeral snow have somewhat reduced the adoption and application of the operational gridded MODIS anisotropy products (BRDF, albedo, and NBAR). In the Inter-Tropical Convergence Zone (ITCZ) dominated regions, for example, clouds may last for several months which results in long gaps in the anisotropy products. Persistent clouds during the monsoon seasons in India and Southeast Asia also contaminate the anisotropy products and limit their utilization. Modelers often prefer to initialize models with snow-free fields and ephemeral snow seasonally covers large areas of North America and Asia. These regions are particularly critical for modeling efforts in light of climate change.

The purpose of this research is to present and evaluate the high quality global, cloud free, seasonally snow free BRDF, albedo, and NBAR products that have been developed for modeling of the Earth's surface radiation and monitoring of the surface vegetation. This gap-filled dataset utilizes the V005 MODIS 30 arc-second (approximately 1 km at the equator) CMG (climate modeling grid) anisotropy products. Previous coarser resolution (1 arc minute) gap-filling efforts had been made with the MODIS V004 albedo product (Moody et al., 2005, 2008) but never with the underlying BRDF product. An initial albedo gap-filling has also been applied to the coarse resolution 0.05° (or 3 arc-minute, about 6 km at the equator) MODIS V005 CMG albedo product (Zhang, 2009). However, here, gap-filling techniques are applied to the three BRDF model parameters and then these gap-filled BRDF model parameters are then used to calculate the appropriate gap-filled, snow-free, white-sky albedo, black-sky albedo and NBAR global products.

2. Data

The operational MODIS BRDF, Albedo, and NBAR algorithm makes use of a linear combination of an isotropic parameter and two kernels (Roujean et al., 1992): the RossThick kernel which is derived from radiative transfer modeling (Ross, 1981), and the LiSparseReciprocal kernel which is based on surface scattering and geometric optical mutual shadowing (Li and Strahler, 1992). The MOD43D CMG product (V005) provides the three kernel weights (ISO, VOL, and GEO) for the RossThick-LiSparseReciprocal model at a 30 arc-second resolution once every 8 days. Data are available for the seven MODIS land bands (0.47 μm, 0.55 μm, 0.67 μm, 0.86 μm, 1.24 μm, 1.64 μm, 2.1 μm) and three broad bands (the shortwave band (0.3–5.0 μm), a visible band (0.3 μm–0.7 μm) and a near-infrared band (0.7–5.0 μm)). Quality Assessment (QA) information for the products in the MCD43D31 dataset and snow flags in the MCD43D34 dataset are provided for each pixel to indicate inversion quality and snow condition.

The primary gap-filling method applied to the BRDF parameter data is based on temporal fitting. When temporal fitting does not produce reliable results, a secondary spatial fit is attempted using the International Geosphere-Biosphere Programme (IGBP) land cover layer from the 500 m yearly V005 MCD12Q1 product (Friedl et al., 2010). The land cover layer is re-projected to a geographic latitude/longitude projection, aggregated to 30 arc-second, and used sparingly for spatial fitting and spatial smoothing in areas of particularly persistent gaps.

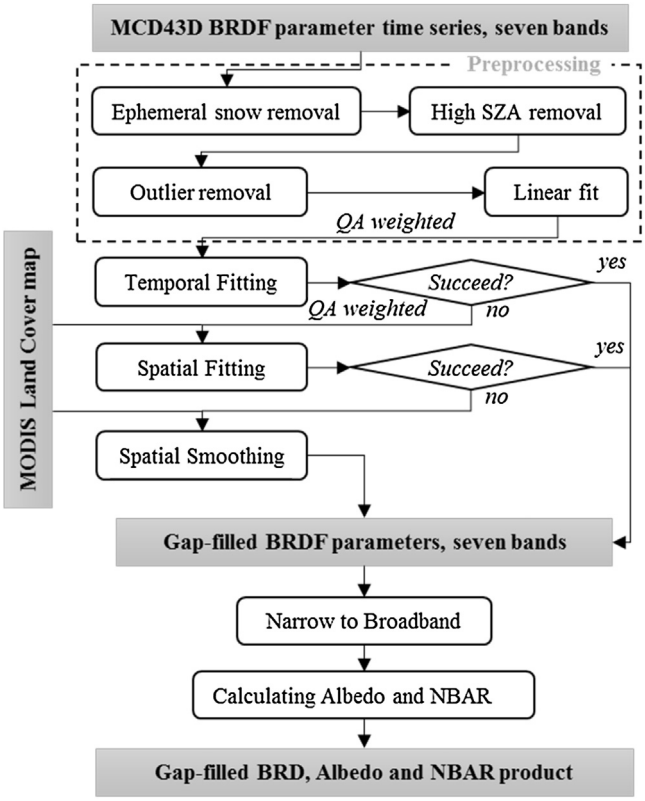

Fig. 1. Flowchart of the gap filling processes.

3. Methods

To create the gap-filled product, we apply temporal fitting techniques, based on vegetation phenology (assisted by spatial fitting techniques), to the global 30arc-second V005 MCD43D CMG BRDF products in order to compensate for missing data and to estimate snow-free situations. We initially apply a temporal fitting method to fill the gaps by creating and fitting each pixel to a one and a half year time series. If the temporal method fails due to limited high quality retrievals, then spatial processes based on land cover mapping are used to fill the gaps with lower quality values. The flowchart is shown in Fig. 1.

3.1. Preprocessing

To generate a snow-free product, pixels with ephemeral snow are removed using the MCD43D34 snow flags (derived from the flags in the original underlying surface relectance data (MO/YD09)). In addition, as the MCD43 products are not recommended for use with solar zenith angles (SZA) beyond 70°, we have removed all of the data for SZA > 70° before initiating the gap filling procedures.

Despite rigorous cloud clearing and atmospheric correction, the original V005 MCD43D products are still contaminated by residual cloud and snow in some regions. This is especially true in the Amazon and in equatorial West Africa, and in high latitude areas. This contamination occurs when the 500 m standard BRDF product

(MCD43A1) is averaged and re-projected to form the 30 arc-second V005 MCD43D parameters. In the averaging process, the quality flag associated with the 30 arc-second average value represents the majority quality of the underlying 500 m pixels. This majority quality assignment strategy works well in most regions of the world, but in some areas (the ITCZ dominated regions for example), the MCD43D pixels flagged as majority high quality may actually still contain some residual cloud contamination, (e.g., one 30 arc-second pixel can still be flagged as majority high quality when it is actually derived from an average of three 500 m high quality pixels and one poor quality cloud contaminated pixel). This allows some residual cloud contamination to persist in the V005 MCD43D product (Note that this effect has been removed in the upcoming Collection V006 MCD43D products by performing an explicit retrieval for the 30 arc-second data with appropriate QA rather than averaging the underlying 500 m data and assigning a majority QA flag).

For V005 however, a median value based outlier removal algorithm (Leys et al., 2013) is applied before the temporal fitting to eliminate these residual cloud and snow contaminated values. Because even values flagged as high quality in the V005 MCD43D may still be contaminated, the outlier removal algorithm is also applied on the high quality values, but with a more conservative threshold to preserve as many of the original high quality values from MCD43D as possible.

3.2. Temporal fit

The software package, TIMESAT was developed to analyze time series of remote sensing data (Jonsson and Eklundh, 2002; Jönsson and Eklundh, 2004). The asymmetric Gaussian fitting method in this package was used to produce spatially and temporally continuous MODIS LAI (Gao et al., 2008) based on seasonal vegetation phenology. In this research, the modified asymmetric Gaussian functions in TIMESAT have been applied to the MCD43D BRDF parameters to compensate for missing data. Much like the resulting albedo and NBAR products, the three BRDF parameters exhibit seasonality (Fig. 2), which is the basis for fitting with the TIMESAT package. The base function of the asymmetric Gaussian model is

$$f(t) \equiv f(t; c_1, c_2, a_1, \ldots, a_5) = c_1 + c_2 \cdot g(t; a_1, \ldots, a_5) \quad (1)$$

Where

$$g(t; a_1, \ldots, a_5) = \begin{cases} \exp\left[-\left(\frac{t-a_1}{a_2}\right)^{a_3}\right], & if\ t > a_1 \\ \exp\left[-\left(\frac{a_1-t}{a_4}\right)^{a_5}\right], & if\ t < a_1 \end{cases} \quad (2)$$

Where c_1 and c_2 represent the base level and the amplitude. a_1 defines the position of the maximum or minimum with respect to the independent time variable t, while a_2 and a_3 determine the width and flatness (kurtosis) when $t > a_1$ (first half of the season), and a_4 and a_5 determine the width and flatness of the second half of the season (Jonsson and Eklundh, 2002).

A total of 76 8-day periods are used to form the time series for the temporal fitting procedure. This includes 46 periods from the processing year of interest, 15 from the end of the previous year, and 15 from the beginning of the following year. This one and a half year time period was chosen to include as many high quality values as possible and reduce failures in the temporal fit. In addition, the one and a half year period ensures the time series data is primarily from the year of interest and avoids the over-smoothing of inter-annual variations that can occur in time series over multiple year.

The temporal fit is driven primarily by the highest quality MCD43D data. However, low quality MCD43D data are also utilized in the initial fitting algorithms. In addition, to avoid a TIMESAT failure due to extended periods of insufficient data due to cloud or ephemeral snow, an initial linear interpolation is employed to fill these no-data intervals. All data are weighted by their QA flags when the asymmetric Gaussian functions are applied, with both the original low quality MODIS data and interpolated data points flagged as low-quality values. This QA flag ensures the overall fit is primarily driven by high quality data and the low quality data only serve as a first guess to condition the temporal fit of the time series. The low quality data will eventually be replaced with the refined estimations from the asymmetric Gaussian functions. However, high-quality data from MCD43D are unchanged during the temporal fitting process (Fig. 2).

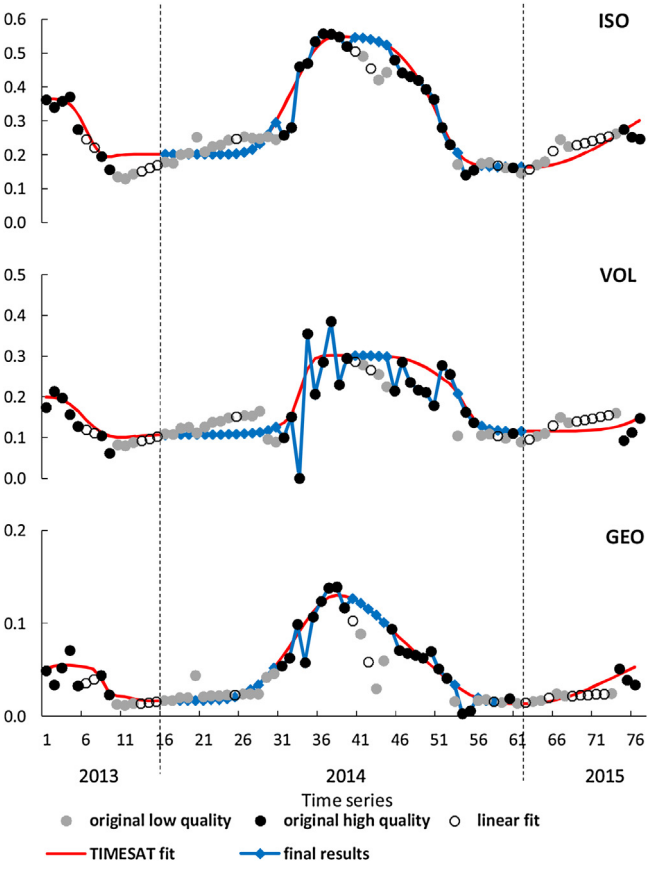

Fig. 2. An example of temporal fit for the three BRDF parameters. This pixel is from the V005 MCD43D NIR band. Note that in V005 MCD43D, only one band of QA is provided. As such, a high quality flag may not always indicate high quality values across all the bands. For example, the time period 33 in this figure is flagged as high quality but may actually be a low quality retrieval. In the V006 all band quality flags will be provided.

In cases where there are only a few valid values within the entire 76 period time series, this temporal fitting process is unable to accurately fill in the gaps. In such cases, initial spatial fits are applied as described in Sections 3.3 and 3.4 and the resultant pixels are flagged accordingly.

3.3. Spatial fit when a temporal fit is not possible

When a spatial fit is necessary, the mean value of the nearby pixels (within 120 rows, or 1° of latitude in the same continent) with the same land cover type is calculated and used as a background time series curve. The no-data pixels are then filled according to this background curve and then adjusted by any actually available data points in the time series. The adjustment is again weighted by the QA of the original data. This method can be only applied to pixels that have at least one valid value in the time series to adjust the

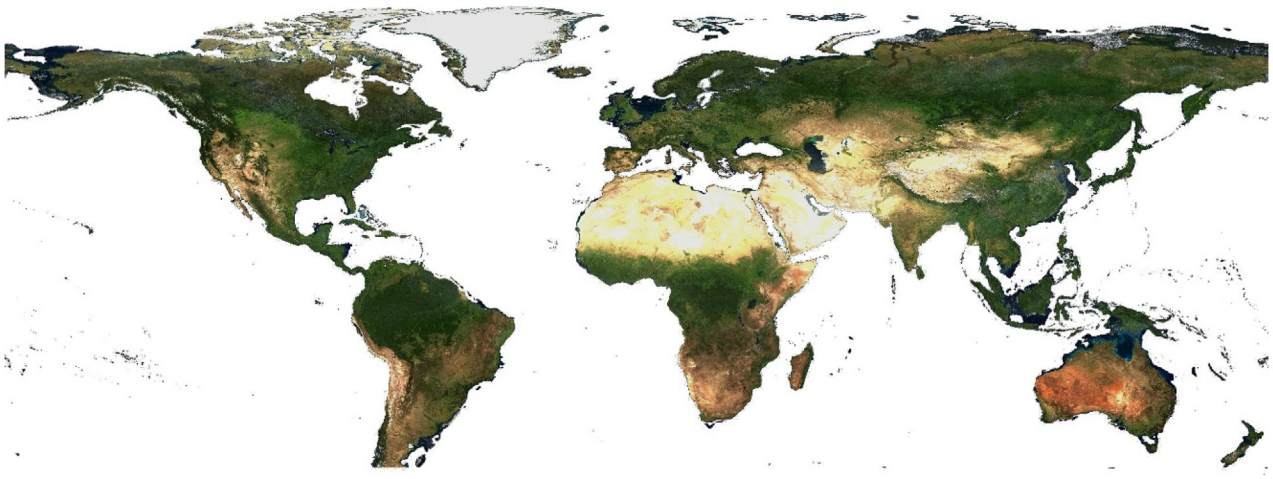

(a)

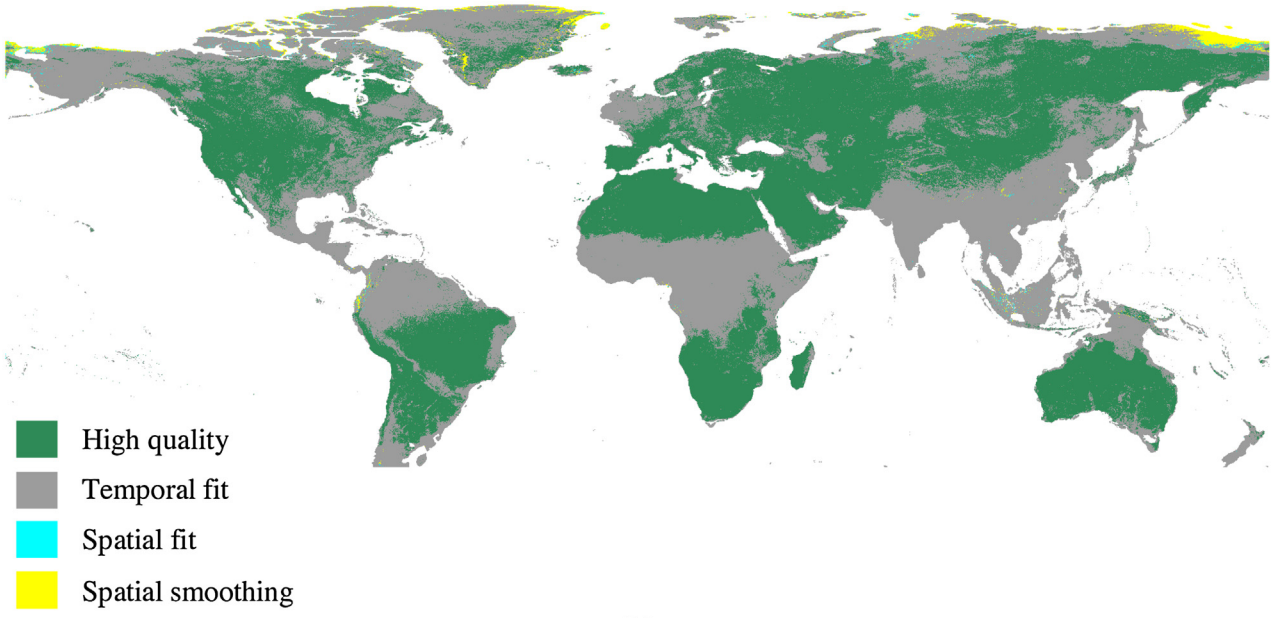

(b)

Fig. 3. (a) Gap-filled, cloud-free, seasonal snow free, true color composite of 30 arc-second white-sky albedo, DOY 193, 2010 and (b) QA flags associated with NIR band (green: high-quality retrievals, gray: temporally fit, cyan: spatially fit, yellow: spatially smoothed). (For interpretation of the references to color in this figure legend, the reader is referred to the web version of this article.)

mean phenology shape from nearby pixels. The spatial fit function is:

$$F = \sum_{i=1}^{n} V_i M_i Wt_i / \sum_{i=1}^{n} M_i M_i Wt_i \quad (3)$$

$$V_j = F * M_j \quad (4)$$

Where F is the adjusting factor, n is the number of available values V_i in the time series, Wt is the weight of the value according to its QA, and M is the mean value of nearby pixels. V_j is the gap in the time series.

3.4. Spatial smoothing

A spatial smoothing method is applied to the pixels that still do not have any data values after the temporal fit and spatial fit. In this step, the no-data pixels are filled by the background value calculated in spatial fit process.

At last, the three broad bands of VIS, NIR, and shortwave parameters are prepared from the gap-filled narrowband BRDF parameters using the narrow-to-broad band coefficients (Liang et al., 1999). The white-sky albedo and black-sky albedo at local solar noon are cal-

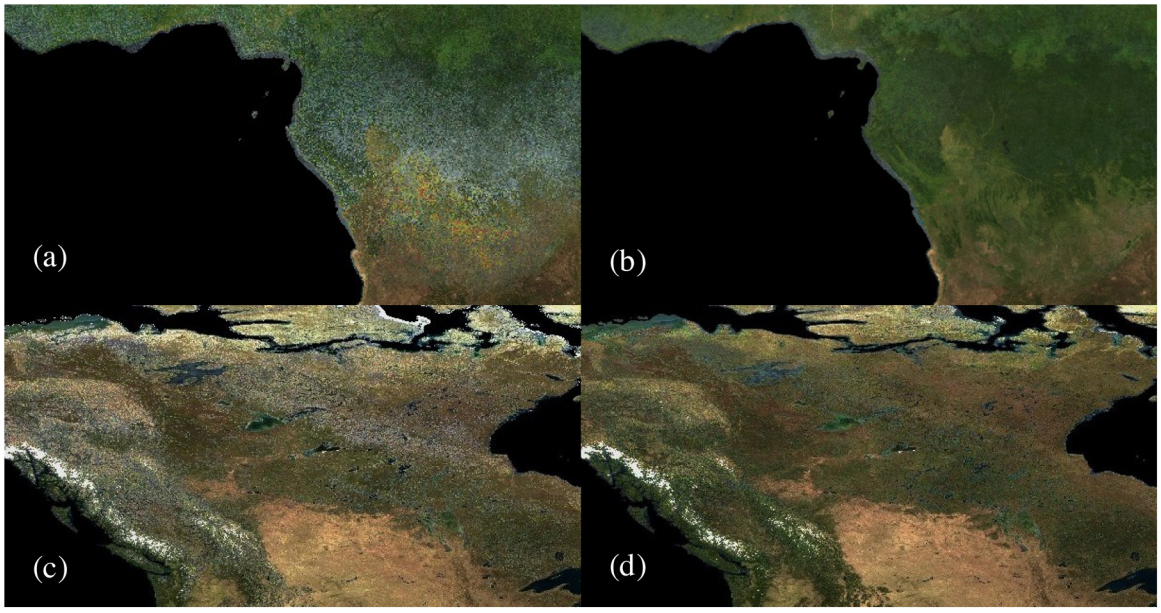

Fig. 4. Cloud and snow contamination removal over Africa (a and b) and North America (c and d). Figures (a) and (c) show gap filled results without the outlier removal method applied, and (b) and (d) show the gap filled results with the outlier removal method applied.

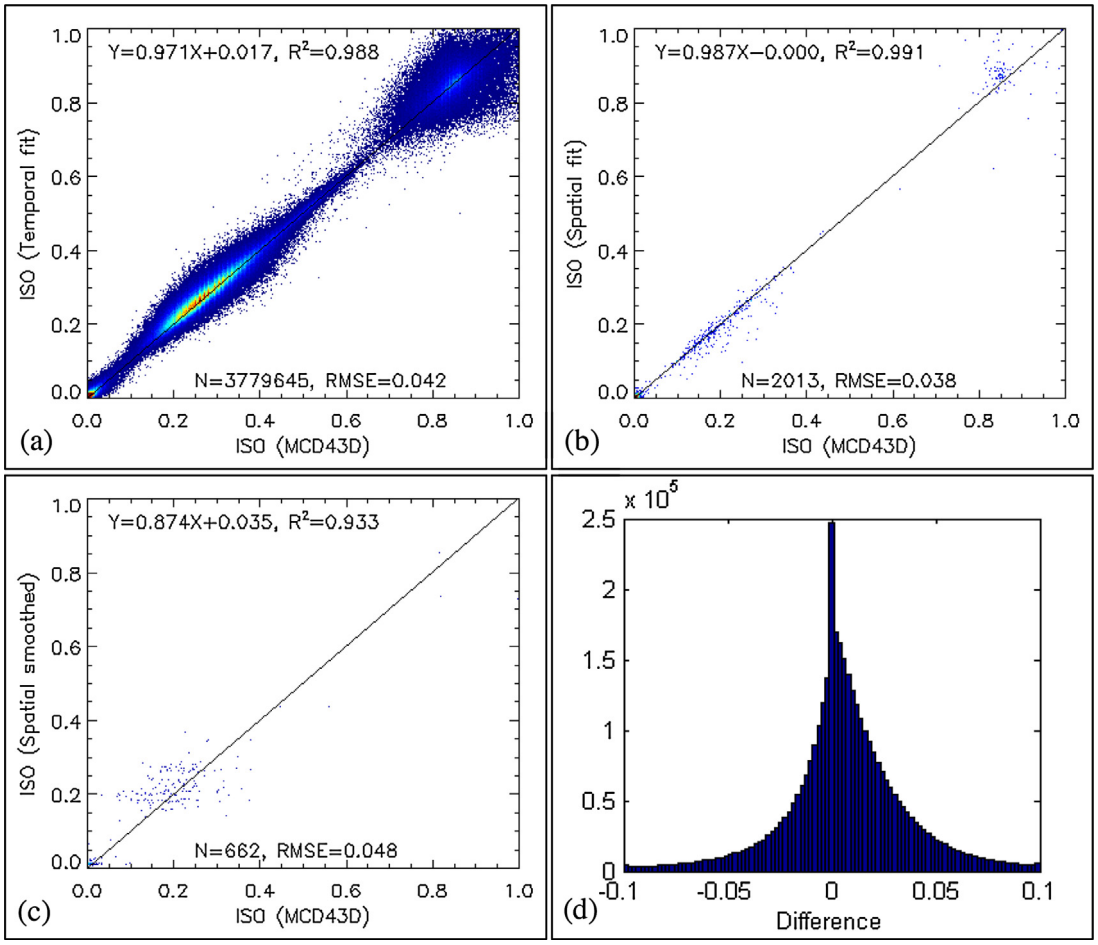

Fig. 5. Original high quality BRDF parameter ISO VS (a): temporally fit, (b): spatially fit, (c): spatially smoothed, and (d): histogram of the gap-filled data minus the original data for the year 2010 (NIR band).

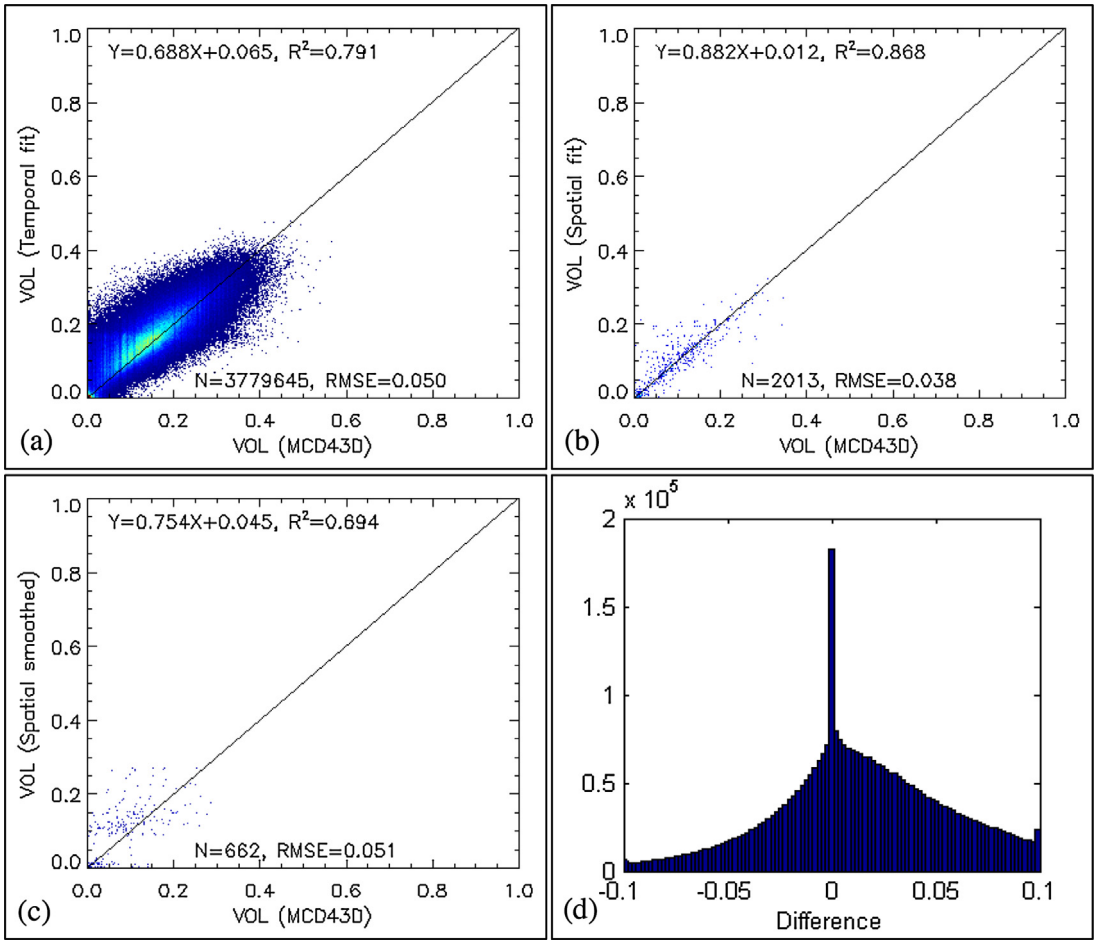

Fig. 6. Original high quality BRDF parameter VOL VS (a): temporally fit, (b): spatially fit, (c): spatially smoothed, and (d): the histogram of the gap-filled data minus the original data for the year 2010 (NIR band).

culated for each narrow band and broad band, and the NBAR at local solar noon is calculated for each narrow band.

Note that actual albedo (or blue-sky albedo) (Lewis and Barnsley, 1994; Román et al., 2010) can be further produced from a combination of the gap-filled white-sky albedo and black-sky albedo with a fraction of diffuse skylight (which can be derived from aerosol optical depth (AOD) data, such as the MOD04 aerosol product (Remer et al., 2005)).

4. Results and evaluation

We have generated a global MODIS gap-filled, seasonal-snow free BRDF, albedo, and NBAR dataset (Fig. 3) at 30 arc-second spatial resolution and 8-day temporal resolution for the entire MODIS era from 2001 to 2015. The aforementioned data layers and associated QA flags indicating the process status are all provided. Most of the areas with gaps can be filled using the temporal fitting procedure (gray areas in Fig. 3b) while the high quality areas remain unchanged (green areas in Fig. 3b).

To evaluate the ability of the initial outlier removal algorithm procedure to identify outliers caused by snow and clouds, two areas are investigated in depth. As previously described, Equatorial Africa often retains residual cloud cover in the original 8-day data. In addition, areas in Canada often retain residual snow cover that was not correctly flagged in the original MCD43D products. The outlier removal method is applied and is shown to remove most of the cloud and snow contaminations in the final gap-filled dataset (Fig. 4). Permanent snow is not removed in this procedure.

Table 1
RMSE between the gap-filled and the original BRDF parameters, WSA, BSA, and NBAR for the NIR (left column) and red bands (right column).

	All gap-filled	Temporal fit	Spatial fit	Spatial smoothing
ISO	0.042, 0.033	0.042, 0.033	0.038, 0.047	0.048, 0.050
VOL	0.050, 0.039	0.050, 0.039	0.038, 0.049	0.051, 0.023
GEO	0.018, 0.012	0.018, 0.012	0.014, 0.014	0.010, 0.007
WSA	0.027, 0.020	0.027, 0.020	0.019, 0.023	0.045, 0.042
BSA	0.025, 0.019	0.025, 0.018	0.018, 0.021	0.045, 0.041
NBAR	0.025, 0.021	0.025, 0.021	0.019, 0.025	0.040, 0.040

To assess the quality of the gap-filled product, we compare the gap-filled values with original high quality values. This comparison was done by randomly selecting 2% of all the land pixels for further analysis. For each selected pixel one high-quality value was randomly removed from the time series and replaced with a fill value. The gap-filling processes were then applied and, for each pixel, the gap-filled BRDF parameters, WSA, BSA and NBAR are compared with the original high quality values for that location. The root-mean-square error (RMSE) (Table 1) and bias (gap-filled minus original) (Table 2) is calculated for band 1 (red) and band 2 (NIR). Since albedo in the NIR band has the largest dynamic range due to vegetation, the discussion below is based on the NIR band.

The gap-filled BRDF parameters reflect an RMSE of around 0.05 for the ISO and VOL parameters, and 0.02 for the GEO parameter. The VOL parameter has the largest prediction error, with an RMSE of around 0.05 and a bias of 0.02 (Tables 1, 2, Fig. 6). Most of the gaps were filled by the temporal fit method so the overall accuracy

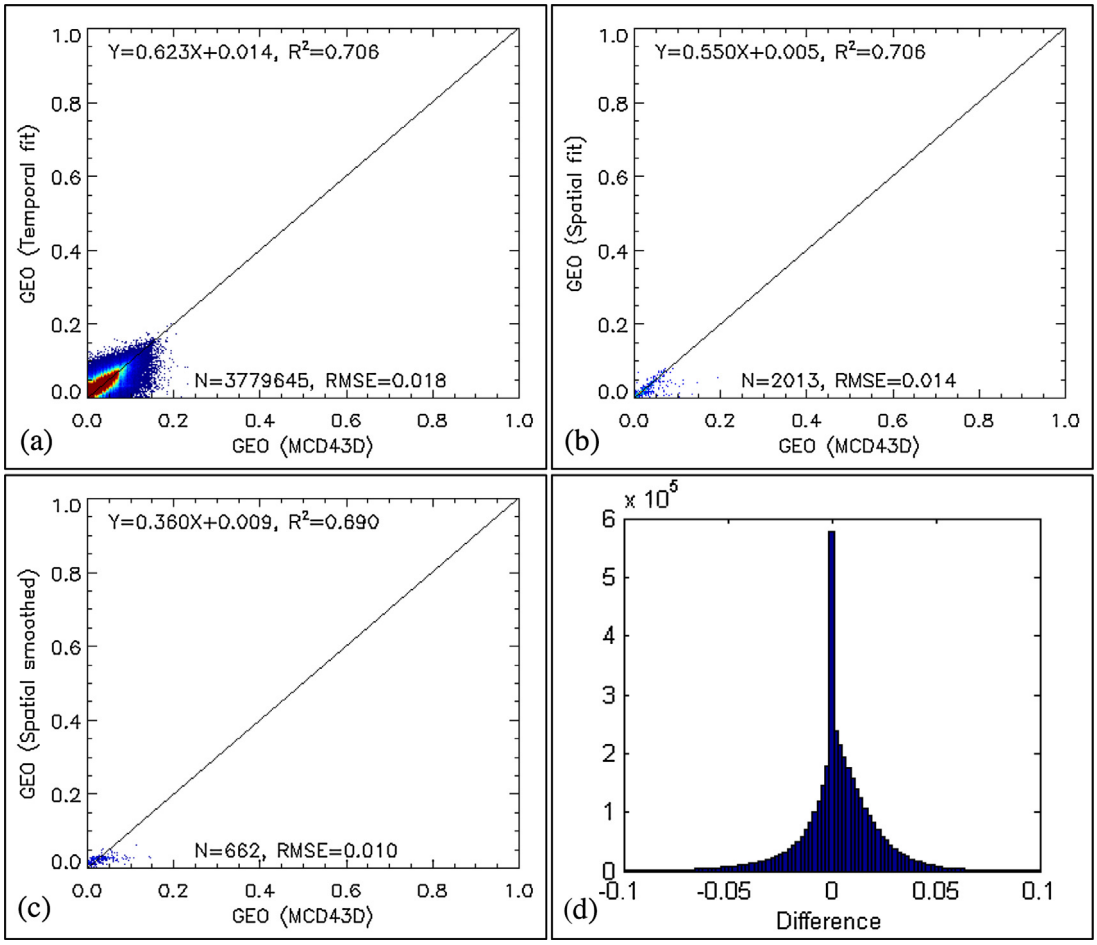

Fig. 7. Original high quality BRDF parameter GEO VS (a): temporally fit, (b): spatially fit, (c): spatially smoothed, and (d): the histogram of the gap-filled data minus the original data for the year 2010 (NIR band).

Table 2
Bias between the gap-filled and the original BRDF parameters, WSA, BSA, and NBAR for the NIR (left column) and red bands (right column).

	All gap-filled	Temporal fit	Spatial fit	Spatial smoothing
ISO	0.005, 0.002	0.005, 0.002	−0.003, −0.011	0.017, −0.020
VOL	0.022, 0.019	0.022, 0.019	0.005, 0.033	0.029, 0.001
GEO	0.003, 0.002	0.003, 0.002	−0.002, −0.004	−0.004, −0.007
WSA	0.005, 0.003	0.005, 0.003	0.001, 0.000	0.028, −0.012
BSA	0.005, 0.003	0.005, 0.003	0.002, 0.003	0.028, −0.011
NBAR	0.002, 0.000	0.002, 0.000	0.000, −0.006	0.020, −0.013

is close to the temporal fit accuracy. Generally, the accuracy for the temporal fit and the spatial fit is higher than the accuracy of spatial smoothing.

We also calculated the WSA, BSA, and NBAR values based on the BRDF parameters, and compared the gap-filled with the original high quality values. The temporally fit results show good accuracy (RMSE 0.025–0.027) with an R-square of 0.99 (Figs. 8–10) as compared to the original high quality data. The RMSE of results from the spatial fit is around 0.019, though relatively few pixels were filled by this process. Most of the histograms of the differences between the total gap-filled albedo and NBAR and the original albedo and NBAR (Figs. 8–10) are almost symmetrical, with the 0 in the center.

The gap-filled BRDF shape is also assessed in comparison to the original high quality BRDF (Fig. 11) retrievals. One pixel was randomly selected for each land cover type from those pixels with a prediction error of 0.027. This threshold was selected as it is the overall standard deviation of the gap-filled data vs. the original data (Table 1). Fig. 11 shows that the BRDF shapes of the gap-filled pixels and the original high quality pixels are close when the view zenith angle is within recommended thresholds (<70°).

To further evaluate the gap-filled data product, we divided the global map horizontally by latitude into 90 parts, with each part a two-degree latitude bin (240 rows). Based on the same randomly selected evaluation data that used for the quantitative analysis (Figs. 5–10), averages of the three BRDF parameters and the white-sky albedo over each two-degree bin were calculated for each land cover type for both the gap-filled (including all the temporally fit, spatially fit, and spatially smoothed) and the original values. Pixels of Croplands, Mixed Forest, Open Shrublands, and Grasslands were evaluated and the gap-filled and original values were compared (Fig. 12). For each selected land cover type, particular latitude bins were chosen according to their spatial distribution to demonstrate the phenology curves (Fig. 13). From these figures it is clear that the gap-filled curves agree well with the original values.

5. Discussion

The temporal fit and spatial fit show better accuracy than the spatial smoothing. The spatial smoothing is the last step to ensure an entirely gap-free product as required by modelers and is expected to provide the poorest quality results since it utilizes the mean value of nearby pixels, directly without adjustment. However, a very limited number of pixels were filled by this method and most of them are concentrated in high latitude areas (Fig. 3). Some of the clusters of spatially smoothed pixels are caused by

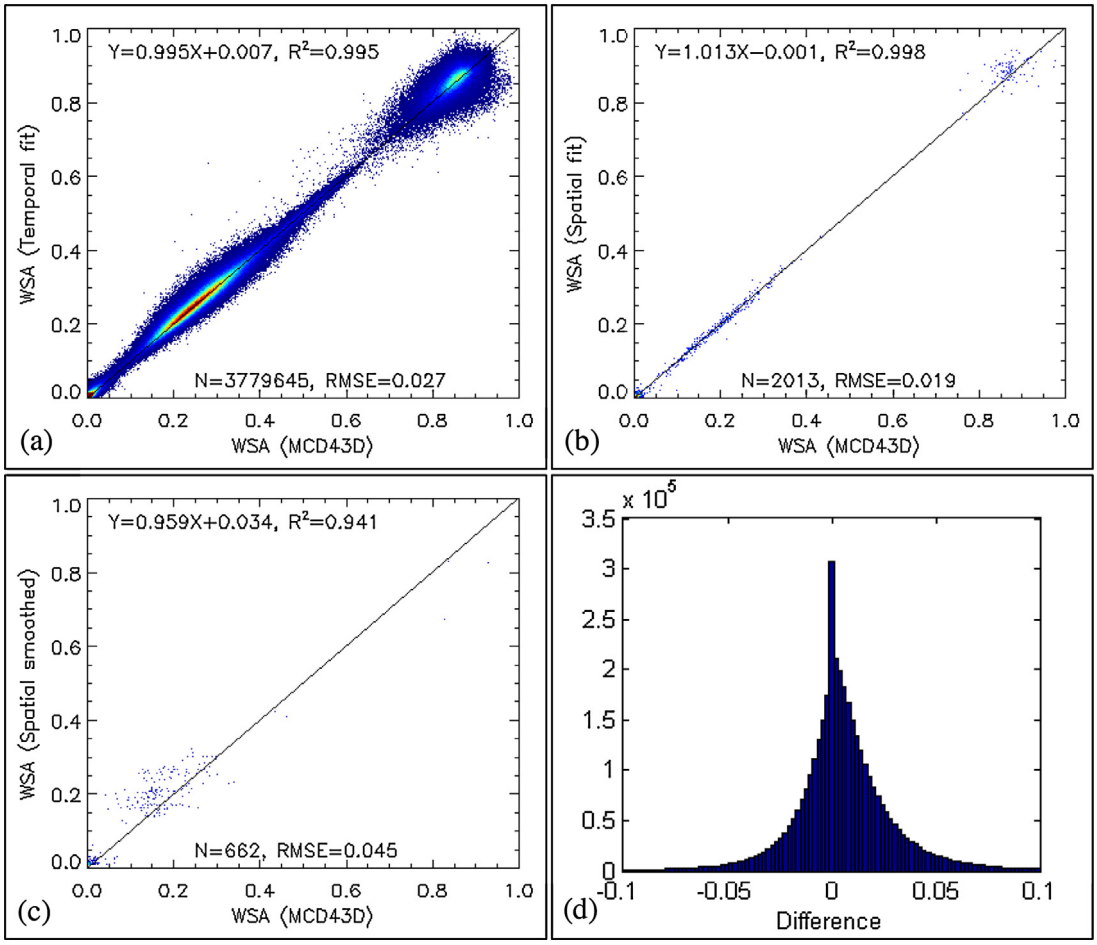

Fig. 8. Original high quality WSA VS (a): temporally fit, (b): spatially fit, (c): spatially smoothed, and (d): the histogram of the gap-filled data minus the original data for the year 2010 (NIR band).

the discrepancy between the MODIS albedo product and the land cover map used. For example, if all of the available time series of a MCD43D pixel indicate it is a snow-albedo, but the land cover map shows it is water (instead of permanent snow), then all the original snow values will be removed and this pixel will be filled by the spatial smoothing method because none of available data points are flagged as water in this time series.

The gap-filling accuracy is higher for the ISO and GEO than the VOL parameter. This may be caused by the more dynamic changes of the volume scattering characteristics of vegetation during the leaf on periods (Fig. 2). We also evaluated the albedo and NBAR derived from the three BRDF parameters, and the results show that the gap-filling accuracy for albedo and NBAR is even higher than the accuracy for the BRDF parameters. Compared with the original high quality data, the overall gap-filling accuracy is 0.027 for the WSA, and 0.025 for the BSA and NBAR.

The gap-filled values agree well with the original data both spatially and temporally (Figs. 12, 13). The gap-filled VOL parameter does not seem to perform quite as well as the ISO and GEO, but it still catches the trends of the original data. And more importantly, the WSA derived from the three gap-filled BRDF parameters agrees well with the original WSA values. Some spikes can be seen in Fig. 12 and these spikes were caused by the uneven distribution of the pixels among the latitude bins. When there are only a few pixels available in a latitude bin (e.g., less than 10), then the mean value can be strongly affected by any errors in the classification map used. The classification map is aggregated from 500 m to 30 arc-second and as such, each land cover type in the 30 arc-second grid represents the majority of the underlying 500 m pixels of the MCD12Q1, a strategy which may induce additional errors. Some large disagreements between the gap-filled values and the original values can be seen on day 001 for Croplands and Open Shrublands at around 5°S (Fig. 12a), on day 185 for Croplands, Open Shrublands, and Grasslands at around 15°N, and for Mixed Forest around 30°N (Fig. 12b). However, all of these large disagreements occur where there were less than 10 pixels available. The curves in Fig. 13 are much smoother and the gap-filled and original values match much better. This is because the particular latitude bin that was selected had the maximum number of pixels for each class so there were plenty of pixels available to calculate the means. There is also a large difference between the gap-filled and the original values for the Croplands at around 20°N where there are relatively more pixels of Crop than for other latitude bins (Fig. 12a). Pixels of cropland in this latitude range are concentrated in the India monsoon region (Fig. 14), which leads to higher chance of pixels being cloud contaminated and fewer high quality values available for the gap-filling. Similarly, the disagreements for Open Shrublands and Grasslands around 15°N (Fig. 12b) can also be caused by the residual cloud contamination from the ITCZ. These disagreements indicate that the VOL parameter is more vulnerable to cloud contamination, and is overestimated when such cloud contamination occurs. This may explain why the gap-filled VOL parameter is sometimes a little bit higher than the original value (remember that the V005 MCD43D is an averaged product and if any of the 4 underlying 500 m pixel was contaminated the result 1 km (or 30 arc-second) value will be affected).

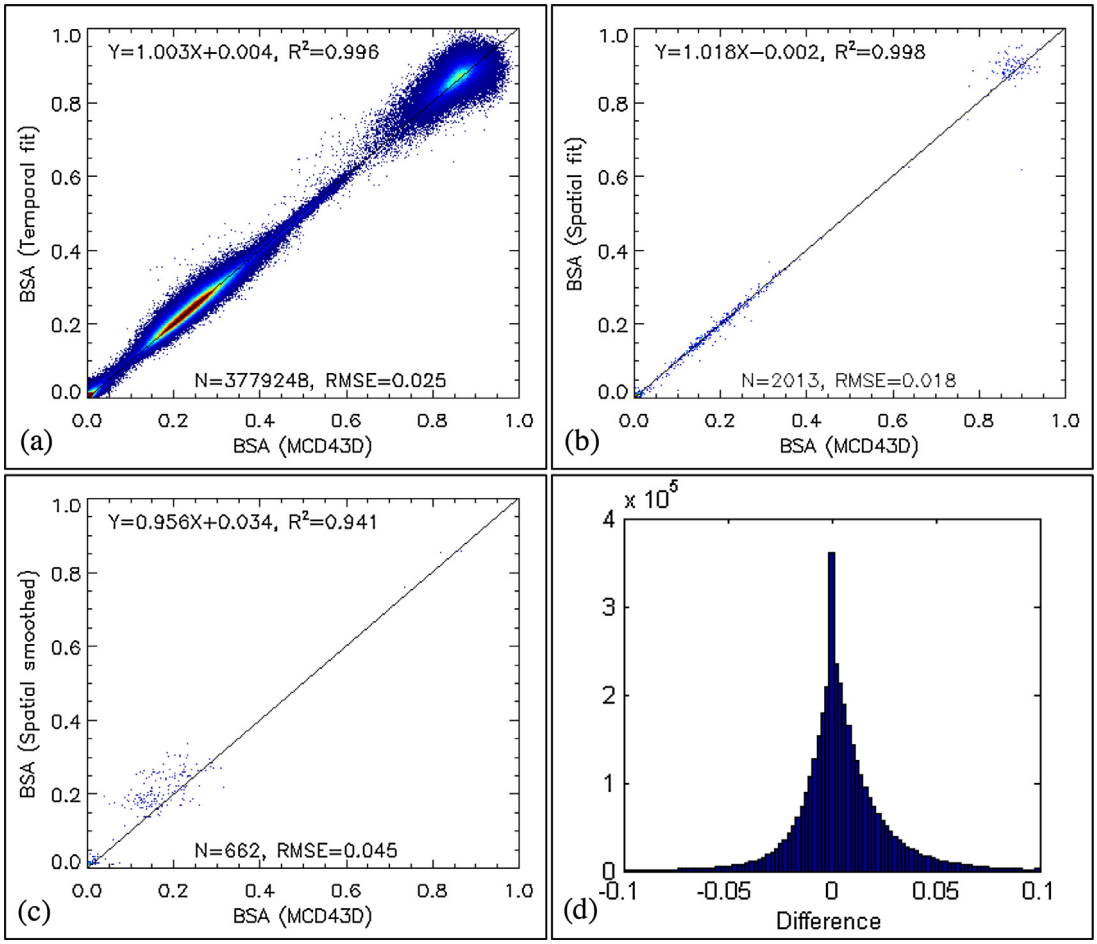

Fig. 9. Original high quality BSA VS (a): temporally fit, (b): spatially fit, (c): spatially smoothed, and (d): the histogram of the gap-filled data minus the original data for the year 2010 (NIR band).

Table 3
RMSE for non-vegetated pixels for the WSA NIR (left column) and red bands (right column). – means no samples were available for evaluation. Snow in this table indicates permanent snow or ice.

RMSE	All gap-filled	Temporal fit	Spatial fit	Spatial smoothing
Water	0.011, 0.010	0.011, 0.010	0.006, 0.007	0.010, 0.008
Wetlands	0.018, 0.008	0.018, 0.008	----, ----	----, ----
Urban	0.017, 0.010	0.017, 0.010	----, ----	----, ----
Snow	0.039, 0.034	0.039, 0.034	0.039, 0.029	0.083, 0.134
Barren	0.014, 0.013	0.014, 0.013	0.006, 0.004	0.032, 0.018

In this work, we use the same gap-filling methods for both vegetated and non-vegetated pixels to avoid implementing a fitting algorithm based specifically on a land cover map. By making this process independent of land cover, we avoid compounding any existing classification errors. In addition, as discussed earlier, the MODIS land cover map has been aggregated from a gridded 500 m map and thus it may include additional classification errors due to this reprojection process. Also note that, non-vegetated pixels typically have low seasonal variations and, consequently, have relatively flat time series. As such, the asymmetric Gaussian function may not work as well on these pixels. Even so, the fitting errors appear to be small as evidenced by the comparison values in Table 3. Even if TIMESAT fails because it cannot detect seasonality, the results of the linear interpolation used in the preprocessing stage would appear to provide sufficiently good results. Another complicating scenario can arise in croplands with multiple cropping cycles. The time series for these regions will have more vegetation cycles than other vegetation types. However, the adapted asymmetric Gaussian function works well on these pixels with a RMSE of 0.028 for the temporal fit for Croplands.

6. Conclusions

Global gap-filled, snow-free BRDF parameters, intrinsic white-sky albedos and black-sky albedos (at local solar noon), and NBAR (MCD43GF) are generated for the years 2001–2015 and can be freely downloaded from our FTP server: ftp://rsftp.eeos.umb.edu/data02/Gapfilled/. Gaps due to clouds and seasonal snow are primarily filled by the use of the asymmetric Gaussian functions in TIMESAT. Additional spatial fitting methods are applied as a last resort to produce a spatially and temporally complete moderate resolution land surface anisotropy dataset.

This gap-filled dataset provides not only the intrinsic albedo of the land surface, but also the gap-filled BRDF parameters. This allows modelers to calculate albedo and surface reflectance at any desired viewing angle and solar zenith angle and derive vegetation indices. The higher temporal resolution of the gap-filled dataset (8-day as opposed to 16-day in the coarser resolution MODIS albedo dataset produced earlier by Moody et al., 2005) provides modelers increased confidence in the product and the flexibility to compute albedo at intervals of only a few days. The higher spatial resolution (30 arc-second) of this dataset, as compared to the gap-filled datasets of 1 arc min (Moody et al., 2005), and of 3 arc min (Zhang, 2009), is closer to the scale of ground measurements and is more useful for describing the dynamics of change on the Earth's surface.

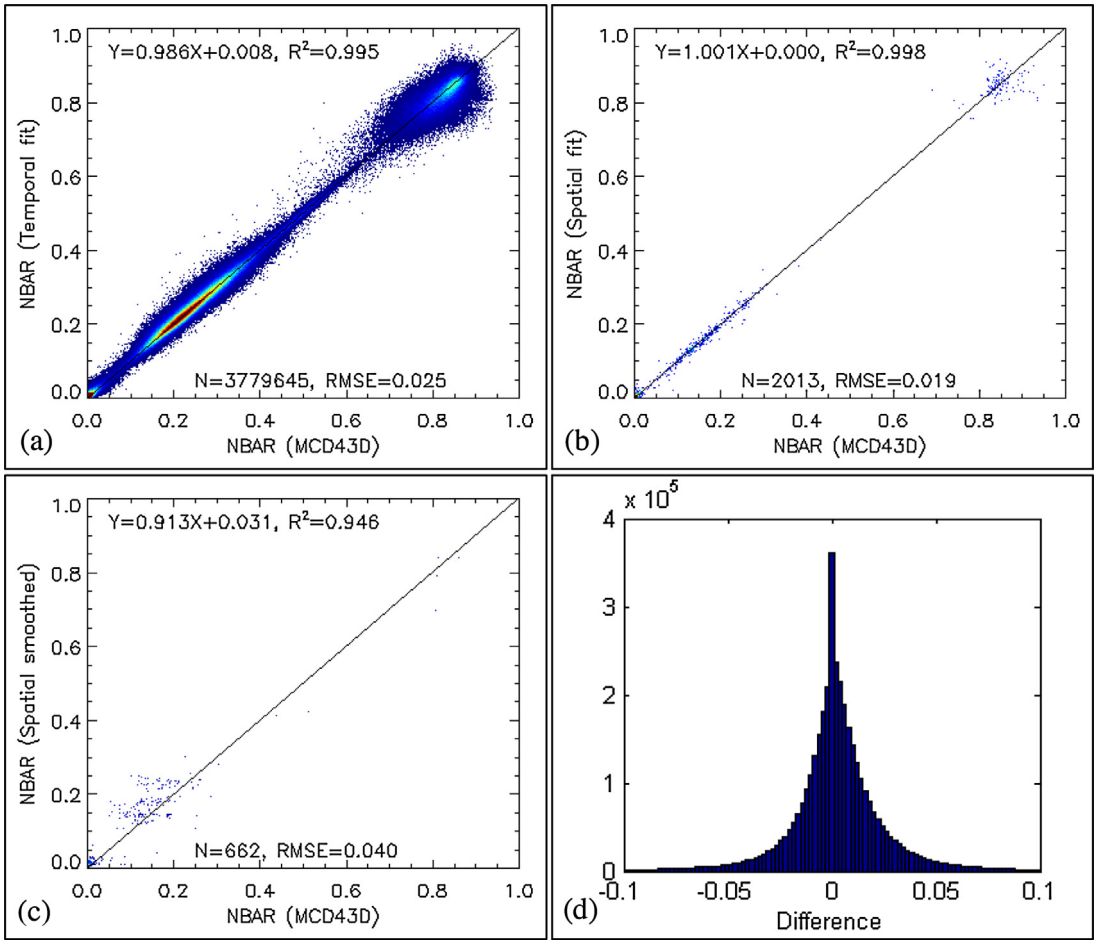

Fig. 10. Original high quality NBAR VS (a): temporally fit, (b): spatially fit, (c): spatially smoothed, and (d): the histogram of the gap-filled data minus the original data for the year 2010 (NIR band).

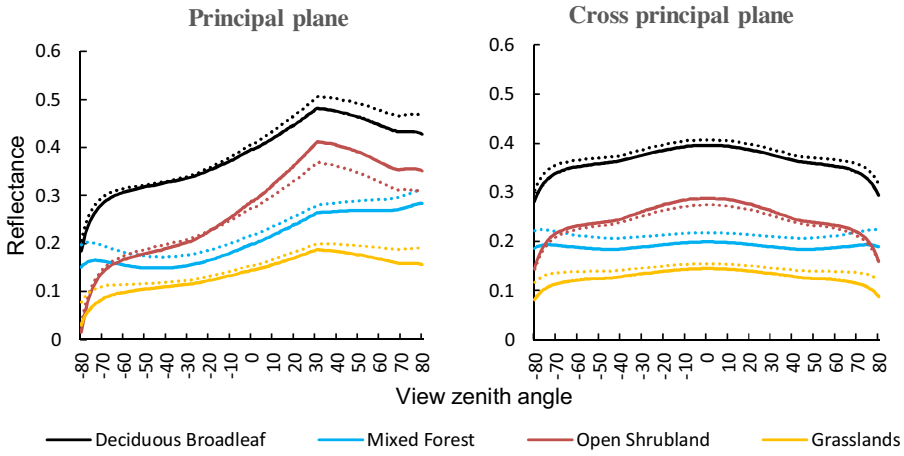

Fig. 11. BRDF shapes for the original high quality data (solid lines) vs. the gap-filled values (dashed lines) for randomly selected pixels with a prediction error of 0.027. The solar zenith angle is 30°.

The spatially and temporally complete snow-free BRDF, Albedo and NBAR values have been largely developed for global modelers who require gap-free albedo as an input. However, users should pay strict attention to the QA flags provided (particularly the larger errors and biases of the spatially smoothed data), when using this gap filled dataset.

As previously discussed, the Collection V006 MCD43D is currently being reprocessed as a daily retrieval, and this product uses all clear sky high quality surface reflectances available within each 30 arc-second grid (instead of the method used in V005 MCD43D where the results are averaged from the underlying 500 m BRDF data and assigning a majority QA flag based on the majority QA flags of the underlying data). This strategy will improve the inversion quality associated with the MCD43D product and reduce some of the residual cloud and snow contamination. The development of the gap filling techniques and evaluation strategies for the V005

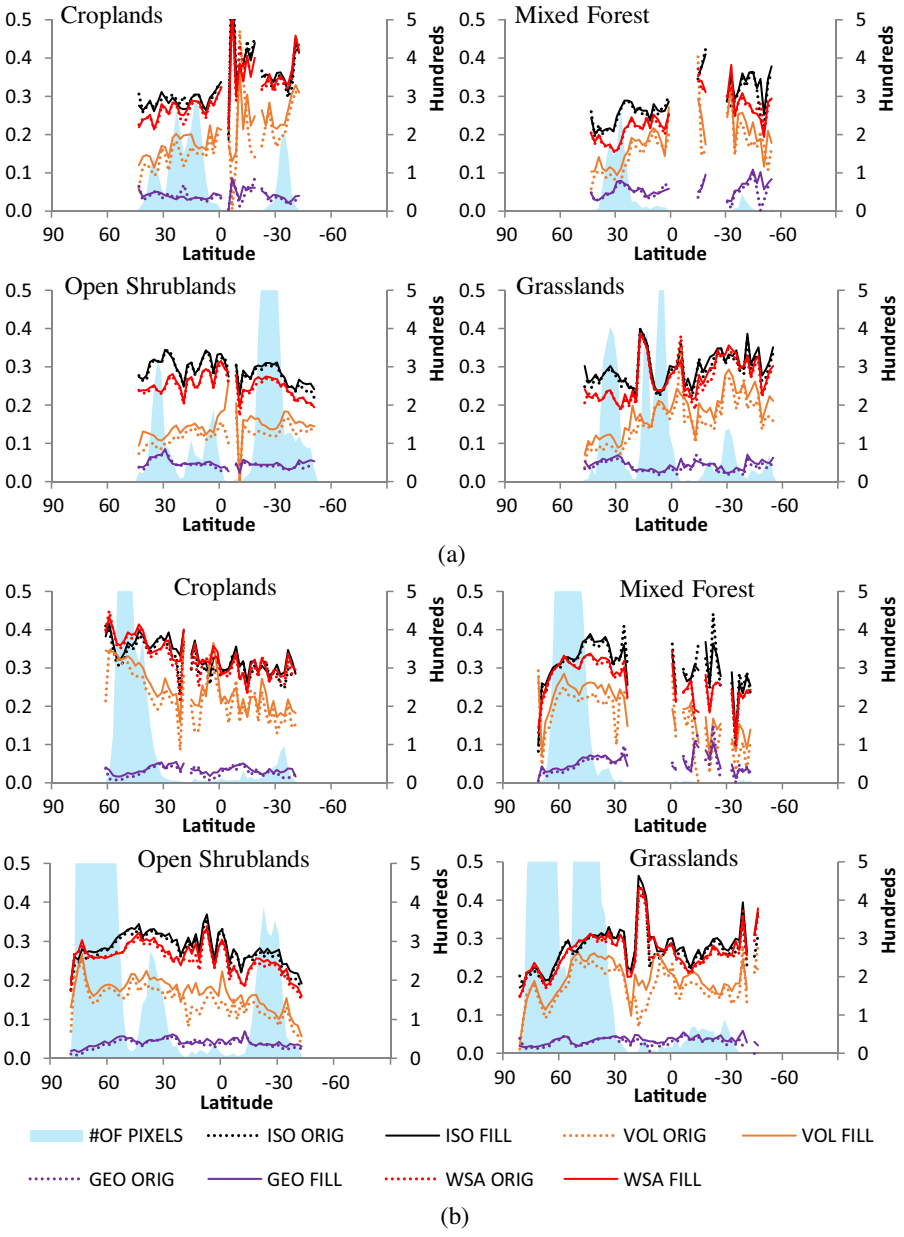

Fig. 12. Mean of the original and gap-filled BRDF parameters and albedo of the NIR band at DOY 001 (a) and 185 (b), in the year 2010 as a function of latitude. Shaded area represents the number of pixels in each latitude bin (secondary vertical axis).

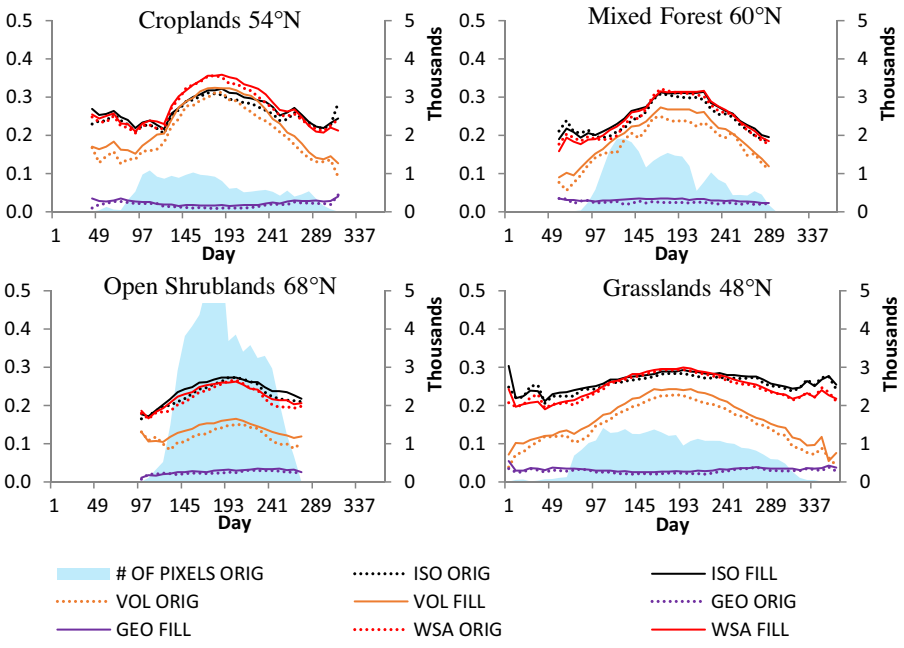

Fig. 13. Means of original and gap-filled white-sky albedos in the NIR band in 2010 as a function of day of year for specific latitude bins (note 60°N represents the latitude bin 58–60°). Shaded area represents the number of pixels in each latitude bin (secondary vertical axis).

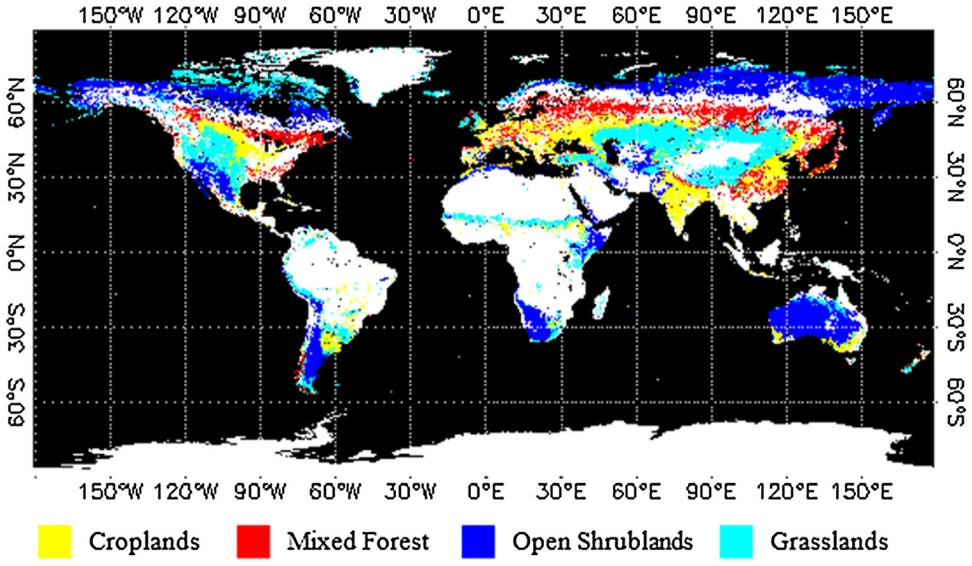

Fig. 14. Spatial distribution of the selected classes in the classification map.

product, however, will be applicable to the future production of a gap-filled data set from the daily V006 MCD43D product as well. We will start to produce the gap-filled V006 MCD43D when the operational processing of the MCD43D is completed.

Acknowledgments

The authors would like to thank Dr. Jonsson and Dr. Eklundh who developed the open source software TIMESAT. Drs. Feng Gao, Qingling Zhang, and Eric Moody all served as pathfinders in the production of gap filled products. This work was supported by NASA NNX11AD58G, NNX12AL38G and NNX14AI73G.

References

Campagnolo, M.L., Sun, Q., Liu, Y., Schaaf, C., Wang, Z., Román, M.O., 2016. Estimating the effective spatial resolution of the operational BRDF, albedo, and nadir reflectance products from MODIS and VIIRS. Remote Sens. Environ. 175, 52–64, JOUR.

Cescatti, A., Marcolla, B., Santhana Vannan, S.K., Pan, J.Y., Román, M.O., Yang, X., Schaaf, C.B., et al., 2012. Intercomparison of MODIS albedo retrievals and in situ measurements across the global FLUXNET network. Remote Sens. Environ. 121, 323–334, http://dx.doi.org/10.1016/j.rse.2012.02.019.

Charney, J., Quirk, W.J., Chow, S., Kornfield, J., 1977. A comparative study of the effects of albedo change on drought in semi-arid regions. J. Atmos. Sci., http://dx.doi.org/10.1175/1520-0469(1977)034<1366:ACSOTE>2.0.CO;2.

Chopping, M., Schaaf, C.B., Zhao, F., Wang, Z., Nolin, A.W., Moisen, G.G., Bull, M., et al., 2011. Forest structure and aboveground biomass in the southwestern United States from MODIS and MISR. Remote Sens. Environ. 115 (11), 2943–2953, http://dx.doi.org/10.1016/j.rse.2010.08.031.

Dickinson, R.E., Hanson, B., 1984. Vegetation-albedo feedbacks. Clim. Processes Clim. Sensit., 180–186, JOUR.

Diner, D.J., Martonchik, J.V., Borel, C., Gerstl, S.A.W., Gordon, H.R., Knyazikhin, Y., Verstraete, M.M., et al., 2008. Multi Angle Imaging Spectro-Radiometer (MISR): Level 2 Surface Retrieval Algorithm Theoretical Basis. JPL D-11401, Revision E. GEN. Jet Propulsion Laboratory (JPL/NASA), Pasadena, 78 p.

d'Entremont, R.P., Schaaf, C.B., Lucht, W., Strahler, A.H., 1999. Retrieval of red spectral albedo and bidirectional reflectance using AVHRR HRPT and GOES

satellite observations of the New England region. J. Geophys. Res.: Atmos. 104 (D6), 6229–6239, JOUR.
Friedl, M.A., Sulla-Menashe, D., Tan, B., Schneider, A., Ramankutty, N., Sibley, A., Huang, X., 2010. MODIS Collection 5 global land cover: algorithm refinements and characterization of new datasets. Remote Sens. Environ. 114 (1), 168–182, JOUR.
Gao, F., Morisette, J.T., Wolfe, R.E., Ederer, G., Pedelty, J., Masuoka, E., Nightingale, J., et al., 2008. An algorithm to produce temporally and spatially continuous MODIS-LAI time series. IEEE Geosci. Remote Sens. Lett. 5 (1), 60–64, JOUR.
Glanz, H., Carvalho, L., Sulla-Menashe, D., Friedl, M.A., 2014. A parametric model for classifying land cover and evaluating training data based on multi-temporal remote sensing data. ISPRS J. Photogramm. Remote Sens. 97, 219–228, JOUR.
Hautecœur, O., Leroy, M.M., 1998. Surface bidirectional reflectance distribution function observed at global scale by POLDER/ADEOS. Geophys. Res. Lett. 25 (22), 4197–4200, JOUR.
Hill, M.J., Averill, C., Jiao, Z., Schaaf, C.B., Armston, J.D., 2008. Relationship of MISR RPV parameters and MODIS BRDF shape indicators to surface vegetation patterns in an Australian tropical savanna. Can. J. Remote Sens. 34 (sup2), S247–S267, JOUR.
Hill, M.J., Román, M.O., Schaaf, C.B., Hutley, L., Brannstrom, C., Etter, A., Hanan, N.P., 2011. Characterizing vegetation cover in global savannas with an annual foliage clumping index derived from the MODIS BRDF product. Remote Sens. Environ. 115 (8), 2008–2024, JOUR.
Hill, M.J., Román, M.O., Schaaf, C.B., 2012. Dynamics of vegetation indices in tropical and subtropical savannas defined by ecoregions and Moderate Resolution Imaging Spectroradiometer (MODIS) land cover. Geocarto Int. 27 (2), 153–191, JOUR.
Hill, M.J., Zhou, Q., Sun, Q., Schaaf, C.B., Southworth, J., Mishra, N.B., Crews, K.A., et al., 2016. Dynamics of the relationship between NDVI and SWIR32 vegetation indices in southern Africa: implications for retrieval of fractional cover from MODIS data. Int. J. Remote Sens. 37 (6), 1476–1503, JOUR.
Hu, B., Lucht, W., Strahler, A.H., Schaaf, C.B., Smith, M., 2000. Surface albedos and angle-corrected NDVI from AVHRR observations of South America. Remote Sens. Environ. 71 (2), 119–132, JOUR.
Jönsson, P., Eklundh, L., 2004. TIMESAT—a program for analyzing time-series of satellite sensor data. Comput. Geosci. 30 (8), 833–845, JOUR.
Jiao, Z., Hill, M.J., Schaaf, C.B., Zhang, H., Wang, Z., Li, X., 2014. An anisotropic flat index (AFX) to derive BRDF archetypes from MODIS. Remote Sens. Environ. 141, 168–187, JOUR.
Jonsson, P., Eklundh, L., 2002. Seasonality extraction by function fitting to time-series of satellite sensor data. IEEE Trans. Geosci. Remote Sens. 40 (8), 1824–1832, JOUR.
Kala, J., Evans, J.P., Pitman, A.J., Schaaf, C.B., Decker, M., Carouge, C., Sun, Q., et al., 2014. Implementation of a soil albedo scheme in the CABLEv1. 4b land surface model and evaluation against MODIS estimates over Australia. Geosci. Model Dev. 7 (5), 2121–2140, JOUR.
Lacaze, R., Maignan, F., 2006. POLDER-3/PARASOL Land Surface Algorithms Description. GEN, POSTEL.
Lawrence, P.J., Chase, T.N., 2007a. Climate Impacts on the Community Climate System Model (CCSM 3.0) of Making the Surface Hydrology of the Community Land Model (CLM 3.0) Consistent with the Simple Biosphere Model (SiB 2.0). CIRES, Boulder, Colorado, pp. 35, JOUR.
Lawrence, P.J., Chase, T.N., 2007b. Representing a new MODIS consistent land surface in the community land model (CLM 3.0). J. Geophys. Res.: Biogeosci. 112 (G1) (JOUR).
Lawrence, P.J., Chase, T.N., 2010. Investigating the climate impacts of global land cover change in the community climate system model. Int. J. Climatol. 30 (13), 2066–2087, JOUR.
Leroy, M., Deuze, J.L., Bréon, F.M., Hautecoeur, O., Herman, M., Buriez, J.C., Roujean, J.L., et al., 1997. Retrieval of atmospheric properties and surface bidirectional reflectances over land from POLDER/ADEOS. J. Geophys. Res.: Atmos. 102 (D14), 17023–17037, JOUR.
Lewis, P., Barnsley, M.J., 1994. Influence of the sky radiance distribution on various formulations of the earth surface albedo. In: 6th International Symposium on Physical Measurements and Signatures in Remote Sensing, ISPRS, CONF, CNES Val d'Isere, France, pp. 707–715.
Leys, C., Ley, C., Klein, O., Bernard, P., Licata, L., 2013. Detecting outliers: do not use standard deviation around the mean, use absolute deviation around the median. J. Exp. Soc. Psychol. 49 (4), 764–766, JOUR.
Li, X., Strahler, A.H.1, 1992. Geometric-optical bidirectional reflectance modeling of the discrete crown vegetation canopy: effect of crown shape and mutual shadowing. IEEE Trans. Geosci. Remote Sens. 30 (2), 276–292, JOUR.
Liang, S., Strahler, A.H., Walthall, C., 1999. Retrieval of land surface albedo from satellite observations: a simulation study. J. Appl. Meteorol. 38 (6), 712–725, JOUR.
Liang, S., Jin, Y., Lucht, W., Schaaf, C.B., Gao, F., Li, X., Strahler, A.H., 2003. Consistency of MODIS surface BRDF/Albedo retrievals 1. Algorithm Perform., JOUR.
Lucht, W., Schaaf, C.B., Strahler, A.H., 2000. An algorithm for the retrieval of albedo from space using semiempirical BRDF models. IEEE Trans. Geosci. Remote Sens. 38 (2), 977–998, JOUR.
Lucht, W., Prentice, I.C., Myneni, R.B., Sitch, S., Friedlingstein, P., Cramer, W., Smith, B., et al., 2002. Climatic control of the high-latitude vegetation greening trend and Pinatubo effect. Science 296 (5573), 1687–1689, JOUR.
Martonchik, J.V., Diner, D.J., Crean, K.A., Bull, M.A., 2002. Regional aerosol retrieval results from MISR. IEEE Trans. Geosci. Remote Sens. 40 (7), 1520–1531, JOUR.
Martonchik, J.V., 1997. Determination of aerosol optical depth and land surface directional reflectances using multiangle imagery. J. Geophys. Res.: Atmos. 102 (D14), 17015–17022, JOUR.
Moody, E.G., King, M.D., Platnick, S., Schaaf, C.B., Gao, F., 2005. Spatially complete global spectral surface albedos: value-added datasets derived from Terra MODIS land products. IEEE Trans. Geosci. Remote Sens. 43 (1), 144–158, JOUR.
Moody, E.G., King, M.D., Schaaf, C.B., Platnick, S., 2008. MODIS-derived spatially complete surface albedo products: spatial and temporal pixel distribution and zonal averages. J. Appl. Meteorol. Climatol. 47 (11), 2879–2894, JOUR.
Morcrette, J.J., Barker, H.W., Cole, J.N.S., Iacono, M.J., Pincus, R., 2008. Impact of a new radiation package, McRad, in the ECMWF integrated forecasting system. Mon. Weather Rev. 136 (12), 4773–4798, JOUR.
Myhre, G., Kvalevåg, M.M., Schaaf, C.B., 2005. Radiative forcing due to anthropogenic vegetation change based on MODIS surface albedo data. Geophys. Res. Lett. 32 (21), JOUR.
Oleson, K.W., Bonan, G.B., Schaaf, C., Gao, F., Jin, Y., Strahler, A., 2003. Assessment of global climate model land surface albedo using MODIS data. Geophys. Res. Lett. 30 (8), JOUR.
Privette, J.L., Eck, T.F., Deering, D.W., 1997. Estimating spectral albedo and nadir reflectance through inversion of simple BRDF models with AVHRR/MODIS-like data. J. Geophys. Res.: Atmos. 102 (D24), 29529–29542, JOUR.
Rahman, H., Pinty, B., Verstraete, M.M., 1993. Coupled surface-atmosphere reflectance (CSAR) model: 2. Semiempirical surface model usable with NOAA advanced very high resolution radiometer data. J. Geophys. Res.: Atmospheres 98 (D11), 20791–20801, JOUR.
Remer, L.A., Kaufman, Y.J., Tanré, D., Mattoo, S., Chu, D.A., Martins, J.V., Kleidman, R.G., et al., 2005. The MODIS aerosol algorithm, products, and validation. J. Atmos. Sci. 62 (4), 947–973, JOUR.
Roesch, A., Schaaf, C., Gao, F., 2004. Use of moderate-resolution imaging spectroradiometer bidirectional reflectance distribution function products to enhance simulated surface albedos. J. Geophys. Res.: Atmos. 109 (D12), JOUR.
Román, M.O., Schaaf, C.B., Lewis, P., Gao, F., Anderson, G.P., Privette, J.L., Barnsley, M., et al., 2010. Assessing the coupling between surface albedo derived from MODIS and the fraction of diffuse skylight over spatially-characterized landscapes. Remote Sens. Environ. 114 (4), 738–760, JOUR.
Ross, J.v, 1981. The Radiation Regime and Architecture of Plant Stands 3. BOOK, Springer Science & Business Media.
Roujean, J., Leroy, M., Deschamps, P., 1992. A bidirectional reflectance model of the Earth's surface for the correction of remote sensing data. J. Geophys. Res.: Atmos. 97 (D18), 20455–20468, JOUR.
Roy, D.P., Zhang, H.K., Ju, J., Gomez-Dans, J.L., Lewis, P.E., Schaaf, C.B., Kovalskyy, V., et al., 2016. A general method to normalize Landsat reflectance data to nadir BRDF adjusted reflectance. Remote Sens. Environ. 176, 255–271, JOUR.
Sütterlin, M., Schaaf, C.B., Stöckli, R., Sun, Q., Hüsler, F., Neuhaus, C., Wunderle, S., 2015. Albedo and reflectance anisotropy retrieval from AVHRR operated onboard NOAA and MetOp satellites: algorithm performance and accuracy assessment for Europe. Remote Sens. Environ. 168, 163–176, http://dx.doi.org/10.1016/j.rse.2015.06.023.
Salomon, J.G., Schaaf, C.B., Strahler, A.H., Gao, F., Jin, Y., 2006. Validation of the MODIS bidirectional reflectance distribution function and albedo retrievals using combined observations from the aqua and terra platforms. IEEE Trans. Geosci. Remote Sens. 44 (6), 1555–1565, JOUR.
Schaaf, C.B., Gao, F., Strahler, A.H., Lucht, W., Li, X., Tsang, T., Roy, D., et al., 2002. First operational BRDF, albedo nadir reflectance products from MODIS. Remote Sens. Environ. 83 (1–2), 135–148, http://dx.doi.org/10.1016/S0034-4257(02)00091-3.
Schaaf, C.B., Martonchik, J., Pinty, B., Govaerts, Y., Gao, F., Lattanzio, A., Taberner, M., et al., 2008. Retrieval of surface albedo from satellite sensors. In: Advances in Land Remote Sensing. CHAP, Springer, pp. 219–243.
Schaaf, C.B., Liu, J., Gao, F., Strahler, A.H., 2011. MODIS albedo and reflectance anisotropy products from Aqua and Terra. In: Land Remote Sensing and Global Environmental Change: NASA's Earch Observing System and the Science of ASTER and MODIS, Remote Sensing and Digital Image Processing Series., pp. 11, 873. article.
Strugnell, N.C., Lucht, W., 2001. An algorithm to infer continental-scale albedo from AVHRR data, land cover class, and field observations of typical BRDFs. J. Clim. 14 (7), 1360–1376, JOUR.
Strugnell, N.C., Lucht, W., Schaaf, C., 2001. A global albedo data set derived from AVHRR data for use in climate simulations. Geophys. Res. Lett. 28 (1), 191–194, http://dx.doi.org/10.1029/2000GL011580.
Wang, Z., Zeng, X., Barlage, M., Dickinson, R.E., Gao, F., Schaaf, C.B., 2004. Using MODIS BRDF and albedo data to evaluate global model land surface albedo. J. Hydrometeorol. 5 (1), 3–14, http://dx.doi.org/10.1175/1525-7541(2004)005<0003:UMBAAD>2.0.CO;2.
Wang, Z., Schaaf, C.B., Lewis, P., Knyazikhin, Y., Schull, M.A., Strahler, A.H., Blair, B.J., et al., 2011. Retrieval of canopy height using moderate-resolution imaging spectroradiometer (MODIS) data. Remote Sens. Environ. 115 (6), 1595–1601, http://dx.doi.org/10.1016/j.rse.2011.02.010.
Wang, Z., Schaaf, C.B., Chopping, M.J., Strahler, A.H., Wang, J., Román, M.O., Shuai, Y., et al., 2012. Evaluation of moderate-resolution imaging spectroradiometer (MODIS) snow albedo product (MCD43A) over tundra. Remote Sens. Environ. 117, 264–280, http://dx.doi.org/10.1016/j.rse.2011.10.002.
Wang, Z., Schaaf, C.B., Strahler, A.H., Chopping, M.J., Román, M.O., Shuai, Y., Fitzjarrald, D.R., et al., 2014. Evaluation of MODIS albedo product (MCD43A) over grassland, agriculture and forest surface types during dormant and

snow-covered periods. Remote Sens. Environ. 140, 60–77, http://dx.doi.org/10.1016/j.rse.2013.08.025.
Wang, Z., Erb, A.M., Schaaf, C.B., Sun, Q., Liu, Y., Yang, Y., Román, M.O., et al., 2016. Early spring post-fire snow albedo dynamics in high latitude boreal forests using Landsat-8 OLI data. Remote Sens. Environ., JOUR.
Wanner, W., Strahler, A.H., Hu, B., Lewis, P., Muller, J.-P., Li, X., Barnsley, M.J., et al., 1997. Global retrieval of bidirectinal reflectance and albedo over land from EOS MODIS and MISR data: theory and algorithm. J. Geophys. Res.–Atmos. 102 (D14), 17143–17161, http://dx.doi.org/10.1029/96JD03295.
Zhang, X.Z.X., Schaaf, C.B., Friedl, M.a., Strahler, a.H., Gao, F.G.F., Hodges, J.C.F., 2002. MODIS tasseled cap transformation and its utility. IEEE Int. Geosci.and Remote Sens. Symp. 2(C, 1063–1065, http://dx.doi.org/10.1109/IGARSS.2002.1025776.
Zhang, X., Friedl, M.A., Schaaf, C.B., Strahler, A.H., Hodges, J.C.F., Gao, F., Huete, A., et al., 2003. Monitoring vegetation phenology using MODIS. Remote Sens. Environ. 84 (3), 471–475, http://dx.doi.org/10.1016/S0034-4257(02)00135-9.
Zhang, X., Tan, B., Friedl, M.A., Goldberg, M.D., Yu, Y., 2012. Long-term Detection of Global Vegetation Phenology from Satellite Instruments. IBOOK, NTECH Open Access Publisher.
Zhang, Q., 2009. A Global Spatially and Temporally Complete Reflectance Anisotropy Database to Improve Surface Characterization for Environmental Modeling. BOOK.
Zhou, L., Dickinson, R.E., Tian, Y., Zeng, X., Dai, Y., Yang, Z., Strahler, A., et al., 2003. Comparison of seasonal and spatial variations of albedos from Moderate-Resolution Imaging Spectroradiometer (MODIS) and Common Land Model. J. Geophysical Res.: Atmos. 108 (D15), JOUR.
Zhou, Q., Hill, M.J., Sun, Q., Schaaf, C.B., 2016. Retrieving understorey dynamics in the Australian tropical savannah from time series decomposition and linear unmixing of MODIS data. Int. J. Remote Sens. 37 (6), 1445–1475, http://dx.doi.org/10.1080/01431161.2016.1154224.
Zoogman, P., Liu, X., Chance, K., Sun, Q., Schaaf, C., Mahr, T., Wagner, T., 2016. A climatology of visible surface reflectance spectra. J. Quant. Spectrosc. Radiat. Transfer 180, 39–46, http://dx.doi.org/10.1016/j.jqsrt.2016.04.003.